Received: 31 October 2019 | Revised: 27 December 2019 | Accepted: 27 December 2019

DOI: 10.1111/jfd.13136

ORIGINAL ARTICLE

Journal of Fish Diseases WILEY

Vertebral column deformity with curved cross-stitch vertebrae in Norwegian seawater-farmed Atlantic salmon, *Salmo salar* L.

Cathrine Trangerud[1] | Håvard Bjørgen[2] | Erling Olaf Koppang[2] | Randi Nygaard Grøntvedt[3] | Hege Kippenes Skogmo[1] | Nina Ottesen[1] | Agnar Kvellestad[2]

[1]Department of Companion Animal Clinical Sciences, Faculty of Veterinary Medicine, Norwegian University of Life Sciences, Oslo, Norway

[2]Section of Anatomy, Faculty of Veterinary Medicine, Norwegian University of Life Sciences, Oslo, Norway

[3]INAQ AS, Trondheim, Norway

Correspondence
Cathrine Trangerud, Department of Companion Animal Clinical Sciences, Faculty of Veterinary Medicine, Norwegian University of Life Sciences, Centrum, P.O. Box 369, N-0102 Oslo, Norway.
Email: cathrine.trangerud@nmbu.no

Funding information
Norwegian Seafood Research Fund, Prevention of cross-stich vertebrae syndrome in farmed Atlantic salmons, Grant/ Award Number: 901430.

Abstract

Pathological changes in the vertebral column of farmed Atlantic salmon in Norway have been reported since the 1990s. Based on the characteristic radiographic findings, we here present a vertebral column deformity named "curved cross-stitch vertebrae" that mainly affects the middle aspect of the vertebral column. Sixty fish, from the west/northwest coast of mid-Norway, were sampled at slaughter and examined by radiography, computed tomography (CT), necropsy, macrophotography, and histology. The vertebral deformities were radiographically graded as mild, moderate, or marked. The main differences between these grades of changes were defined by increased curving of the peripheries of endplates, reduced intervertebral spaces, and vertical displacement of the vertebrae. The curved rims of endplates were located peripheral to a continuous and approximately circular borderline. The CT studies revealed small, multifocal, hypo-attenuating, round to crescent-shaped areas in the notochord, compatible with the presence of gas. Additionally, histology revealed that the axial parts of endplates had circular zones with perforations, through which either notochordal tissue prolapsed into the vertebrae or vascularized fibrochondroid proliferations extended from the vertebrae into the notochord. Inflammation was present in many vertebral bodies. To the best of our knowledge, this is the first report of gas in the notochord of fish.

KEYWORDS

computed tomography, gas, notochord, radiography, spinal deformity

1 | INTRODUCTION

Vertebral deformities are reported in populations of farmed Atlantic salmon (*Salmon salar* L.), with a prevalence ranging from 17% to 73% (Fjelldal, Hansen, & Berg, 2007; Fjelldal et al., 2009; Hansen, Fjelldal, Yurtseva, & Berg, 2010; Witten, Obach, Huysseune, & Baeverfjord, 2006). Several factors have been associated with the development of these conditions, including inadequate phosphorus supply (Baeverfjord et al., 2018; Fjelldal et al., 2009; Sugiura, Hardy, & Roberts, 2004), water temperature (Baeverfjord, Åsgård, & Shearer, 1998; Grini, Hansen, Berg, Wargelius, & Fjelldal, 2011; Takle, Baeverfjord, Lunde, Kolstad, &

Andersen, 2005; Wargelius, Fjelldal, & Hansen, 2005; Ytteborg, Baeverfjord, Torgersen, Hjelde, & Takle, 2010), vaccination (Aunsmo et al., 2008; Berg, Rodseth, Tangeras, & Hansen, 2006; Berg, Yurtseva, Hansen, Lajus, & Fjelldal, 2012; Haugarvoll, Bjerkås, Szabo, Satoh, & Koppang, 2010), and genetic factors (Gjerde, Pante, & Baeverfjord, 2005; McKay & Gjerde, 1986). The prevalence also varies from year to year (Sullivan, Guy, Roberts, & Manchester, 2007).

Most deformities have been identified caudal to the 25th vertebral body (Grini et al., 2011; Hansen et al., 2010; Sullivan, Guy, et al., 2007; Sullivan, Hammond, Roberts, & Manchester, 2007; Wargelius et al., 2005). These deformities have been associated with impaired fillet quality (Haugarvoll et al., 2010; Sullivan, Hammond, et al., 2007) and reduced growth (Gjerde et al., 2005; Hansen et al., 2010). Importantly, the condition may pose a serious animal welfare concern.

Visual examination and palpation of un-eviscerated fish is a method that allows detection of vertebral deformities under farming conditions (Aunsmo et al., 2008; Aunsmo et al., 2009; Gjerde et al., 2005; Grini et al., 2011; Vågsholm & Djupvik, 1998), but radiography is markedly more sensitive and accurate. By radiographical examinations, several types of vertebral deformities have been described, such as platyspondyly, fusion, dislocation, and reduced or increased mineralization (Boglione et al., 2013; Fjelldal et al., 2007, 2012; Helland et al., 2006; Kvellestad, Høie, Thorud, Tørud, & Lyngøy, 2000). The earlier lack of a standardized classification of the different vertebral deformities in Atlantic salmon has in part been addressed by the improved ordering system proposed by Witten et al. (Witten, Gil-Martens, Huysseune, Takle, & Hjelde, 2009). Additionally, a review by Boglione et al. further standardized the terminology (Boglione et al., 2013).

In 2016, a new manifestation of vertebral deformity of unknown aetiology was identified in Norwegian seawater-farmed salmon (G. Bæverfjord, pers. com.). Based on radiographs, the observed abnormally shaped vertebrae were temporarily termed "cross-stitch vertebrae," with similarities to previously published changes (Fjelldal et. al, 2007; Martens, Obach, Ritchie, & Witten, 2005).

Here, we further investigated aspects of this novel vertebral deformity by applying radiography and computed tomography (CT). The radiological findings were compared with pathological changes observed macroscopically, and by macrophotography and histology.

2 | MATERIALS AND METHODS

2.1 | Animals

Sixty Atlantic salmons, from four different commercial locations of the west/northwest coast of Norway, were included in the study. The fish in these locations had previously been reported to suffer from the cross-stitch vertebral deformity. The fish characterized by proportionally shorter bodies and a plump appearance as compared with other fish in the same populations were selected as they were expected to be affected. Thirty-five visually normal and 25 visibly shorter fish were included in the present study (Table 1). In addition, 10 fish from a location without any known history of such vertebral deformities were sampled as additional controls. Samplings were performed from January 2018 to March 2019. Euthanasia was performed according to national regulations. The fish were subsequently transported on ice, overnight, to the Faculty of Veterinary Medicine, Norwegian University of Life Sciences, in Oslo. Radiography, computed tomography (CT), and necropsy were performed the following day.

TABLE 1 Numbers of fish within each category sampled at slaughter line according to presampling agreement

Visual category at slaughter	History of presence in farms harbouring fish with changes in the vertebral column				
	Loc 1	Loc 2	Loc 3	Loc 4	Total
Normal	10	10	10	5	35
Short	10	5	5	5	25

Note: Locations 1–4 with histories of affected fish.

2.2 | Imaging

Radiographic examinations were performed using a direct digital system (SoundEklin eSeries DR) at 63 kVp, 10 mAs. The fish were radiographed in right lateral recumbency, and three of the fish were additionally radiographed in ventrodorsal projection. The CT images were acquired using a 4-detector row CT scanner (BrightSpeed, GE Healthcare), using a 1.25-mm slice thickness and 0.625-mm overlap, with helical acquisition in bone and soft tissue algorithms. The fish were positioned ventrally. Radiographs and CT studies were reviewed by three observers. Individual body length (tip of the snout to the base of the caudal fin) was determined using the CT images.

The deformities were radiographically categorized into mild, moderate, or marked, and normal if no changes were observed. The main differences between mild, moderate, and marked changes were increased curving of the endplates, reduced intervertebral space, and vertical dislocation of the vertebral bodies. The curving of the peripheral rim of the endplates varied from mild (decreased degree of concavity) to marked (incurving of the opposing endplate). Although all three categories of deformity could be present in the same fish, one category was often predominant. The number of dots per inch (dpi) in radiographs was increased by factors of about 2 and 6, and in CT images, by a factor 4, for publishing.

2.3 | Necropsy

All fish were necropsied. The left lateral skeletal muscle of the body was removed to expose the vertebral column and abdominal organs for inspection and sampling. Whole columns or cranial plus caudal segments were fixed in 10% phosphate-buffered formalin or were trypsinized.

2.4 | Histology

Based on evaluations during field sampling, and obtained by radiography, CT, and necropsy, vertebral columns were selected for histological examination. They were decalcified in 10% hydrochloric acid (Chemi-Teknik AS) for 3 days and subsequently stored in formalin. Thereafter, vertebrae (nos. 1–46 or more) of columns from three individuals were cut in the median plane into right and left halves. Cranial (vertebrae nos. 1–10) and caudal (vertebrae nos. 25–34) segments of columns from three additional individuals were divided by cutting in the median, transverse, or horizontal (level of central axis) planes. These section surfaces were photographed.

Vertebrae or parts thereof were prepared for histology by dehydration in a graded ethanol series, cleared in xylene, and embedded

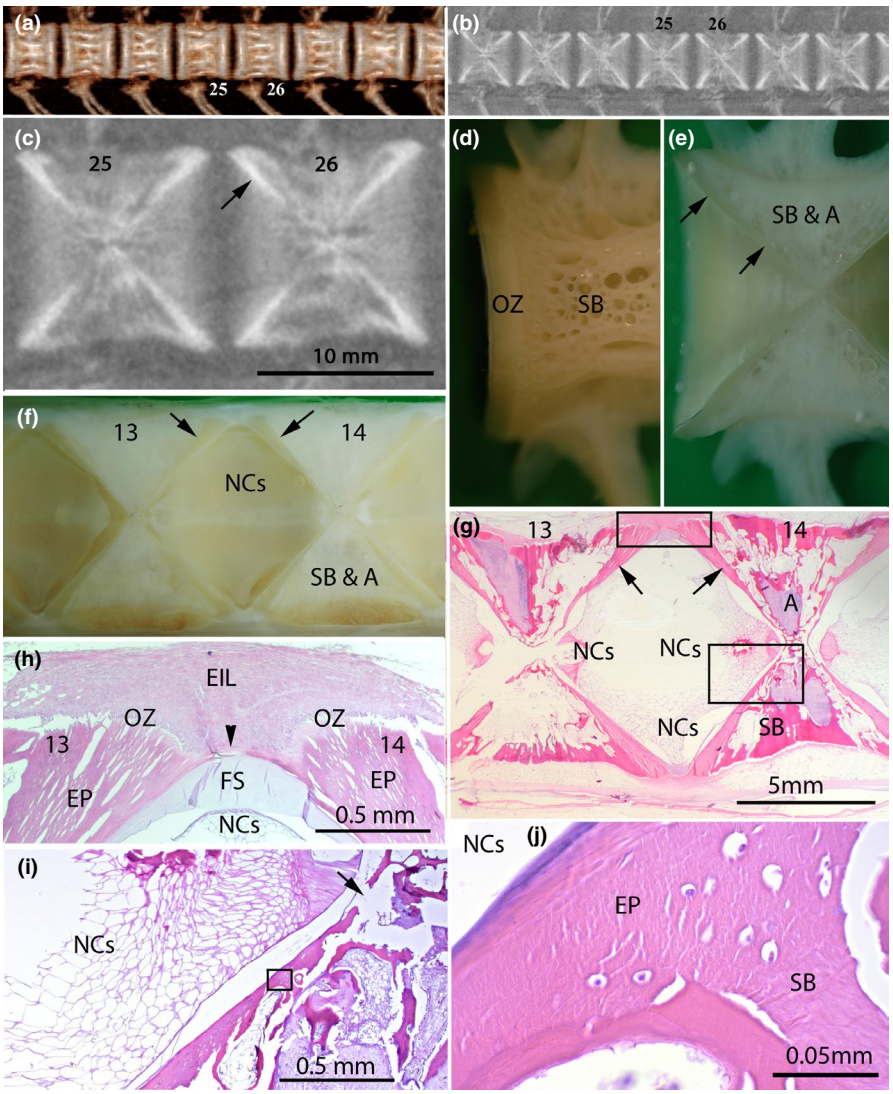

FIGURE 1 Vertebral columns with apparently no radiographical and no pathological changes. (a) 3D computed tomography showing vertebrae 22–28 with regular intervertebral spaces. (b) and (c) radiographs from the same segment, depicting well-aligned vertebral bodies that are separated by radiolucent and regular intervertebral spaces. The vertebral bodies consist of axially located compact bone (arrow), divided into cranial and caudal endplates (EPs), which have increased opacity, in a cross-stitch-like pattern, and the peripherally located and radiolucent spongiotic bone (SB) and arcualia. (d, e) Vertebra of a column treated with trypsin, formalin-fixed, and decalcified. Macrophotography. (d) Left aspect. Osteogenic zone (OZ) and spongiotic bone (SB). (e) Median aspect of right half with SB and arcualia (A) after cleavage through the median plane. (f) Vertebrae of column fixed in formalin, decalcified, and divided in the median plane. Opposing endplates (EPs, arrows), notochordal cells (NCs). Macrophotography. (g–j) Haematoxylin and eosin (H&E)-stained histological section. External intervertebral ligament (EIL). Axial to the EPs and EIL is the internal periosteal ligament (IPL, arrowhead) and fibrous sheath (FS). NCs are located axial to the FS. (h) Greater detail of the area within the upper rectangle in (g). (i) Greater detail of the area within the lower rectangle in (g), showing the approximate place affected by axial-located pathology depicted in other figures. The discontinuity (arrow) is assumed to represent a section artefact because the endplates become progressively thinner toward the axis. (j) Greater detail of the area within the rectangle in (i), including bridging between the EP and SB. All images are oriented with the cranial direction to the left. Vertebrae are numbered if the same vertebrae are present in more than one photograph. All the histological sections are stained with H&E.

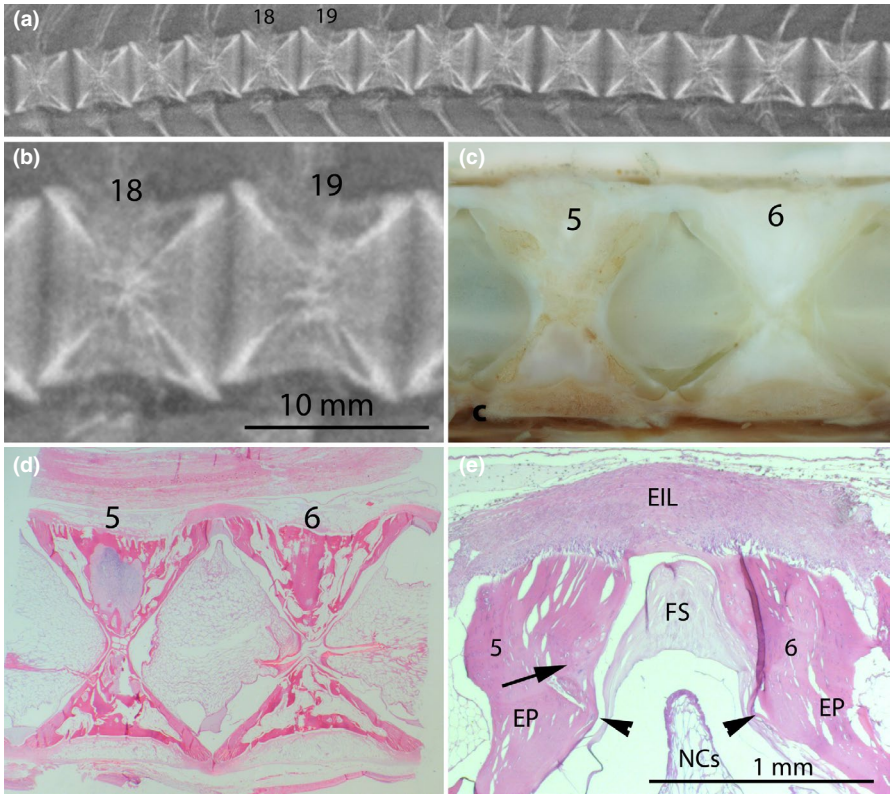

FIGURE 2 Representative example of mild curved cross-stitch vertebral deformity. (a) and (b) radiographs. Changes are characterized by a faintly visible curving of the peripheral rims of the endplates (EPs), reduced intervertebral space, and mild vertical displacement and contact with the opposing endplate. Macrophotography (c) and haematoxylin and eosin (H&E)-stained section (d) of two vertebral bodies, detailed in (e). Peripheral rims in the dorsal parts of the opposing EPs have a more peripherally directed growth. (e) Points of altered directions are marked with arrowheads. A sparse amount of chondroid tissue is also seen in the EPs (arrow). Notochordal cells (NCs)

in paraffin according to a standard protocol (Bancroft & Gamble, 2008). Sectioning started approximately from the above-mentioned cut surfaces. Sections were stained with haematoxylin and eosin (H&E) according to a standard protocol (Bancroft & Gamble, 2008) and examined by light microscopy.

2.5 | Trypsinization

A cranial and a more caudal segment from each of two individuals, one with and one without evidence of radiographic deformity, were trypsinized (enzyme diluted in phosphate-buffered saline) until individual vertebrae were separated. The vertebral bodies were photographed both before and after cutting through the median plane, and were subsequently formalin fixed.

2.6 | Statistical analysis

Fish were grouped into visually short and normal (by visual inspection). Significant differences in body length between visibly short and visually normal individuals were verified by Student's *t* test. Body length in cm (from snout to the base of the fin) within each of the four locations, for visually normal and visibly short groups, and grouped according to radiographic diagnosis of the presence or absence of curved cross-stitch vertebrae, is presented as mean with range. Statistical analyses were performed using JMP® Pro 14 software from SAS Institute.

3 | RESULTS

3.1 | Radiographically normal vertebral column

The vertebral body in normal salmon presented radiographically as a uniform and square shape (Figure 1a–c). The compact bone of the vertebral body created a radio-opaque cross, appearing as crossed diagonals, resembling a cross-stitch, which was surrounded by less opaque spongiosa and arcualia. The endplates of the vertebral body were deeply depressed centrally causing a mild biconcave appearance. A radiolucent regular intervertebral space was present between each vertebral body.

3.2 | Curved cross-stitch vertebrae

The vertebral column deformity identified on radiographs and CT showed mild, moderate, or marked changes, including curving of the peripheral rim of the vertebral endplates, with incurving of the opposing endplate, as well as reduced intervertebral spaces (Figures 2a–b, 3, 4a–c and 5). The reduced spaces were associated with displacement between adjacent vertebral bodies without a significant change in the overall linearity of the vertebral column. The two patterns of curving of the most peripheral rims of endplates gave rise to the term "curved cross-stitch vertebrae," which we used hereafter. Five fish with curved cross-stitch vertebrae additionally presented with platyspondyly (Kvellestad et al., 2000).

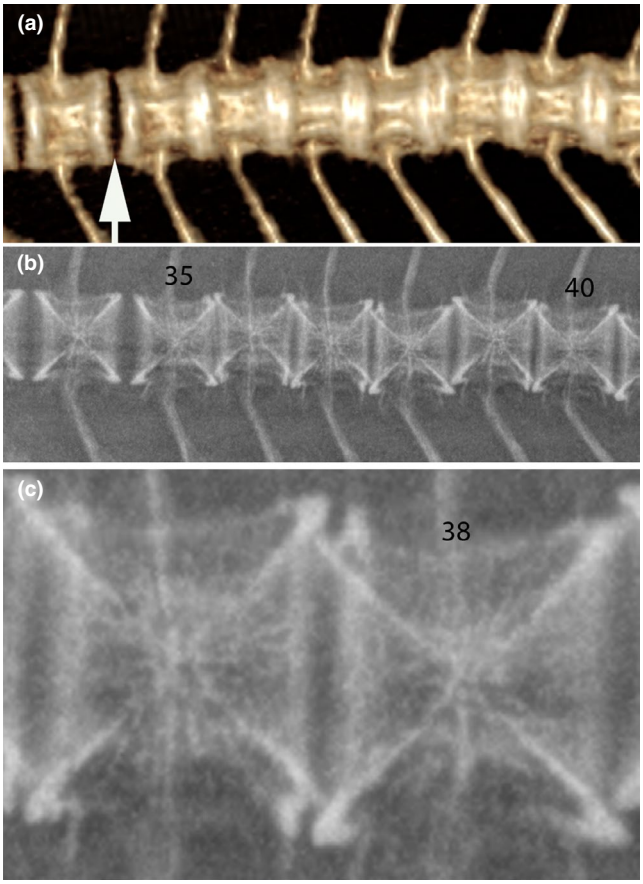

FIGURE 3 Representative example of moderate curved cross-stitch vertebral deformity in segment v35-40. (a) 3D computed tomography (CT) image of segments with reduced of intervertebral spaces and moderate vertical displacement of the vertebral bodies. Visual intervertebral spaces are considered within normal limits (arrow). (b, c) Radiographs. Narrowing of the intervertebral spaces and vertical dislocation of the endplates (EPs) seen on 3D CT. The peripheral rims of the EPs are curved, frequently with one simply curved and the opposing one incurved, forming a curved cross-stitch pattern in both vertebrae

CT studies revealed small, focal, and multifocal hypo-attenuating, round to crescent-shaped areas dorsally, laterally, and ventrally in intervertebral spaces (Figure 5). The Hounsfield units of these hypo-attenuating areas measured up to approximately −1,000 HU and were thus compatible with gas.

This gas was invariably located in connection with curved cross-stitches in the vertebral column; hence, more gas was evident in fish with marked radiographic changes than in those with mild and moderate changes. No gas was detected in any of the radiographically normal fish. The number of individuals within each category and the presence of gas are presented in Table 2.

3.3 | Descriptive statistics

In the specimens overall, curved cross-stitch vertebral changes were observed in 80% of the individuals (48/60) and ranged from 70% to 100% between the four affected fish farms sampled in the study. Vertebral deformities were radiographically seen in all (25/25) visibly short fish and in 66% (23/35) of the visually normal individuals. Gas was detected on CT images in all (25/25) visibly short and in 51% of the visually normal fish (Table 2). Both curved cross-stitch vertebrae and gas were mainly found in the middle aspect of the vertebral column (Figures 6 and 7). Gas was usually found close to the vertebral deformity. The prevalence of gas in fish ranged from 73% to 100% between the four locations. The mean body length in the group with normal vertebrae was 70.5 cm (*SEM* = 1.7), which was significantly greater ($p = .001$) than in the group with vertebral changes (62 cm; *SEM* = 0.8; Table 3). Individual body lengths of fish from the four different locations are presented in Table 4.

3.4 | Necropsy and histology

The anatomy of the vertebral columns with no changes (Figure 1d–j) was in accordance with previous descriptions (François, 1966; Nordvik, Kryvi, Totland, & Grotmol, 2005), and nomenclature in the present study was in accordance with that of Kvellestad et al. (2000). The bend points that arose due to curving of the peripheral rims of endplates were found by morphological methods to locate along a continuous and approximately circular line or border. Metaplastic cartilage was frequently observed in the spaces between the curved rims (Figures 2c–e, 4d–h, 8 and 9). Structures suspected to represent the negative imprint of gas were observed morphologically in the tissue of notochordal cells, which were displaced and flattened (Figure 4d and g).

Most of the endplates with the above-described changes also displayed other changes, which were apparently multifocal and located along a circle with radius approximately 1/5th to 1/4th of the distance from the axis to the periphery of the bodies (Figure 8a). The endplates in several of these locations displayed perforations, through which either notochordal tissue prolapsed into the vertebra's spongiosa, or alternatively, fibrochondroid proliferations extended from the spongiosa into the notochord; in both cases, these were associated with necrotic areas (Figure 8b–d). Most of the proliferations were necrotic but seemed to contain remnants of blood vessels and were also associated with haemorrhages to the notochord. Melano-macrophages and other inflammatory cells were present between the trabeculae of the spongiosa in a moderate number of vertebrae and were apparently associated with the perforations (Figure 9a–b). Inflammatory cells also occurred along the outside of the column and in the interstitial regions in the adjacent skeletal muscle.

4 | DISCUSSION

The present paper describes a deformity in the vertebral column of salmon, termed “curved cross-stitch deformity,” which has not been

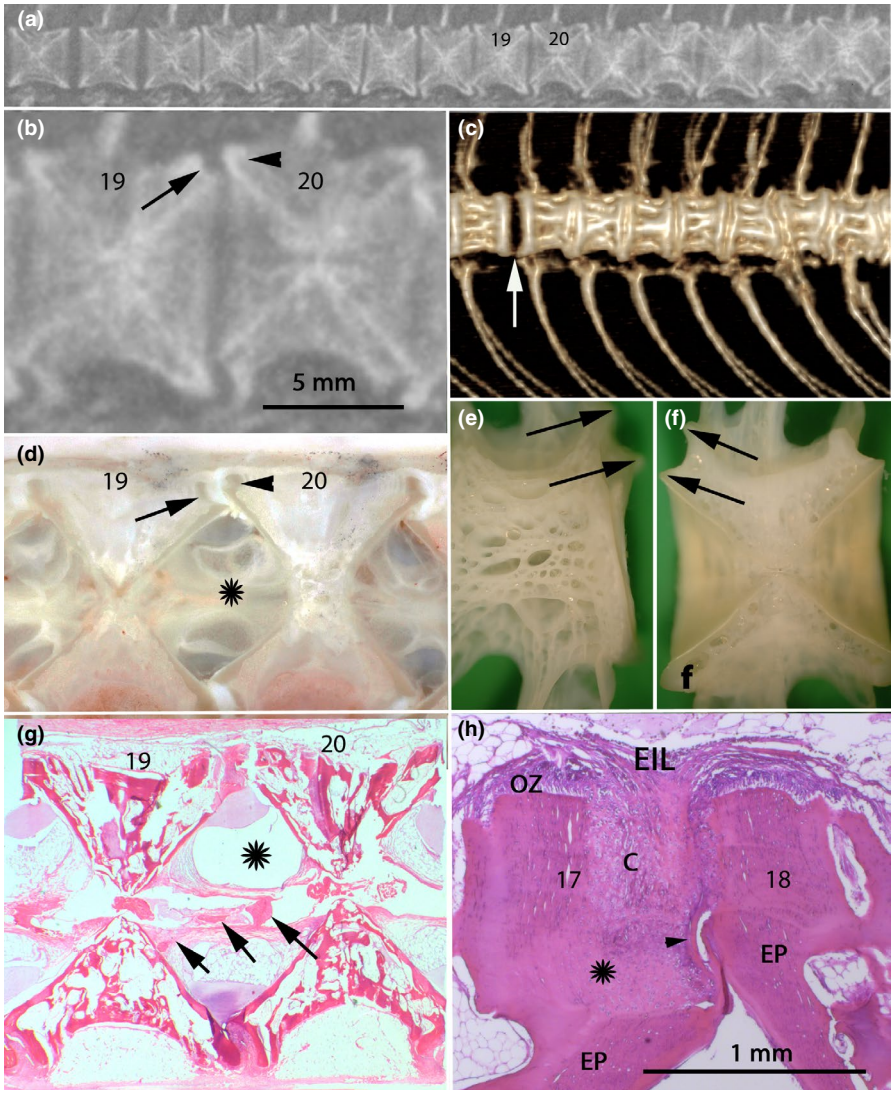

FIGURE 4 Representative example of marked curved cross-stitch vertebral deformity. (a, b) Radiographic changes are comparable to those of moderately curved cross-stitch vertebral deformity but are more extensive. Additionally, dorsal and ventral parts of some vertebral bodies are of unequal length. Changes are characterized by curving of the peripheral rims of endplates (EPs) with simple curving (arrowhead) and incurving of the opposing endplate (arrow). Marked narrowing of the intervertebral spaces and vertical displacement without a significant change in the overall linearity of the vertebral column. (c) Reconstructed 3D CT image, depicting loss of the normal external architecture of the vertebral bodies. An apparently normal vertebral body, and intervertebral space (arrow) to the left. (d) Metaplastic cartilage appears as whitish tissue between the curved rims of opposing EPs, that is, one incurved (arrow) and one simply curved (arrowhead). Gas accumulation (asterisk immediately below the bubble) is seen between the notochordal cells (NCs). Whitish notochord indicates necrosis and distorted structure. (e) The dorsal part of the altered peripheral EP rim (between arrows) is wide and incurved in the caudal direction. It narrows in the ventral direction. (f) The medial aspect shows a similar picture. (g) Gas and necrotic tissue in the notochord are depicted by a bubble (asterisk) and by eosinophilia (intense red colour, arrows), respectively. The structure is also distorted. (h) Detail of peripheral rims of opposing EPs. The left EP is highly incurved with cartilage-like tissue (C) in one place and apparently lacks mineralized tissue in another place (asterisk). The internal periosteal ligament is distorted (arrowhead), whereas the absence of the fibrous sheath (FS) may be artefactual. All except (e) are oriented with the cranial direction to the left

described in detail previously. Curved cross-stitch vertebrae were characterized by significant radiological changes in both visually normal (66%) and visibly shorter fish (100%) and occurred mainly in the middle aspect of the vertebral column. The abnormal vertebrae described in the present study displayed curving of the peripheries of endplates; hence, the term *curved cross-stitch* was employed to reflect both the radiographic and morphological features. In addition, gas was identified in the notochord by CT. Associated changes included perforations in more axial parts of the endplates and inflammation.

The presence of curved cross-stitch vertebrae was significantly associated with the presence of gas on CT. Gas was not identified in any of the radiographically normal fish, which suggests a correlation between gas and the vertebral deformity. The presence of gas is frequently identified on CT studies of humans (Abbas, Hamoud, Peled, & Hershkovitz, 2018; Pfirrmann & Resnick, 2001;

Samartzis et al., 2016) and dogs (Müller, Ludewig, Oechtering, Scholz, & Flegel, 2013; Weber, Berry, & Kramer, 1995) with intervertebral disc disease. The condition has been associated with pain in humans (Belfquih, El Mostarchid, Akhaddar, Gazzaz, & Boucetta, 2014; Gohil, Vilensky, & Weber, 2014). Hence, the findings in the fish with curved cross-stitch could be an animal welfare concern. The distribution and amount of gas identified in these fish are more extensive than that reported in humans and dogs. The reason for this difference between species is unknown and should be further investigated.

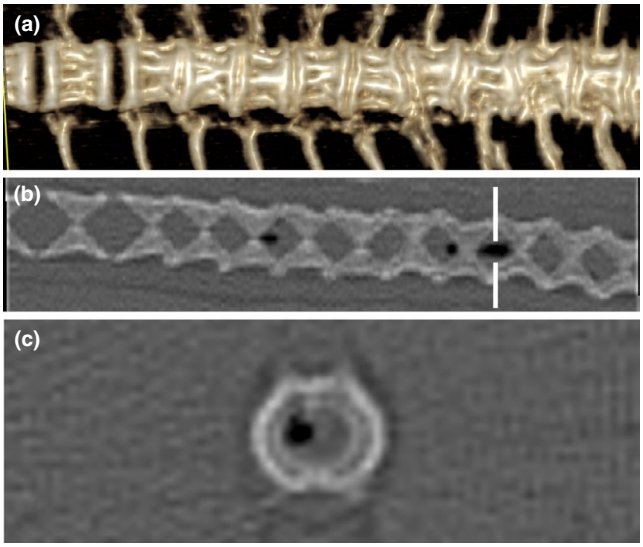

FIGURE 5 Loss of normal external architecture of the vertebral bodies. (a) 3D computed tomography (CT) demonstrating loss of the normal external architecture of the vertebral bodies. An apparently normal whole vertebral body to the left. (b) CT sagittal multiplanar reconstruction. Small and larger, multifocal, hypo-attenuating, round to oval-shaped areas in intervertebral spaces, consistent with the presence of gas in the notochord. (c) CT transverse view. One well-defined, rounded, hypo-attenuating structure, consistent with the presence of gas in the notochord, and a moderately irregular endplate is shown. Localization of (c) is marked with white lines (b)

Similar reduced intervertebral spaces and vertical displacements in slaughter-size Atlantic salmon have been depicted in radiographs from fish sampled in 2003 (Fjelldal et al., 2007, Figures 1c and 2b) and described by radiography and histology in fish sampled in 2001 (Martens et al., 2005; Figures 3 and 4). These changes correspond to types 1 and 17, respectively, by Witten et al., 2009. Additionally, curving is depicted in radiographs of the first study and is described in the second by the term "*inward bending*."

One study on short-tailed salmon (Martens et al., 2005) presented radiographic findings similar to our moderate curved cross-stitch vertebrae. Short-tail salmon often have a high occurrence of deformed vertebrae in the caudal part of the fish (Witten, Gil-Martens, Hall, Huysseune, & Obach, 2005). The different distribution of vertebral changes is likely the cause of different external characteristics of the fish in our study, as compared to short-tail salmon with similar changes. The proportional shortening of the fish in our study is probably related to the distribution of vertebral deformities in the middle part of the vertebral column.

The axial pathological changes observed in the endplates, including perforations at approximately the same distance from the axis, were associated with curved cross-stitch in the examined fish. The detection of curved cross-stitch vertebrae and radiographic

TABLE 2 Visually normal and short fish from locations with histories of affected fish. Number of fish with mild, moderate, and marked changes, based on radiographs

Visual category at slaughter	Radiographic category (number with gas on CT)					
	Normal	Curved cross-stitch				Total
		Mild	Moderate	Marked	Total	
Normal	12 (0)	11 (9)	8 (5)	4 (4)	23 (18)	35 (18)
Short	0	0	3 (3)	22 (22)	25 (25)	25 (25)
Total	12 (0)	11 (9)	11 (8)	26 (26)	48 (43)	60 (43)

Note: The presence of gas diagnosed on computed tomography (CT) images is shown in parentheses.

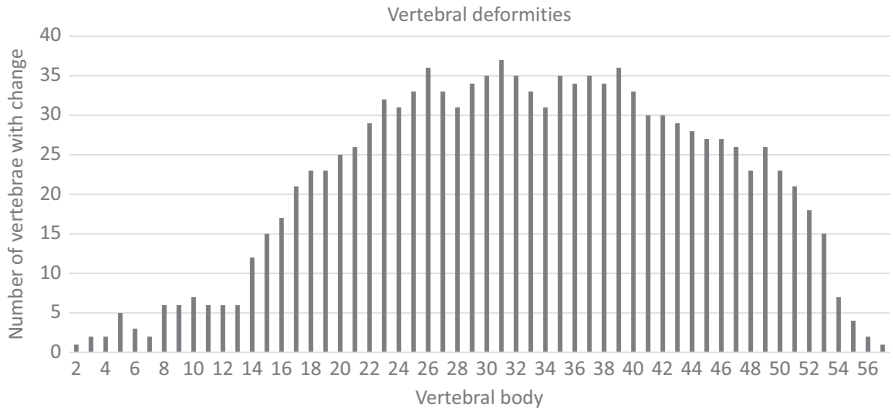

FIGURE 6 Distribution of vertebrae with radiographic changes, consistent with curved cross-stitch vertebrae. The horizontal axis depicts the vertebral number from the cranial to caudal direction. The number of curved cross-stitch vertebrae is shown along the vertical axis

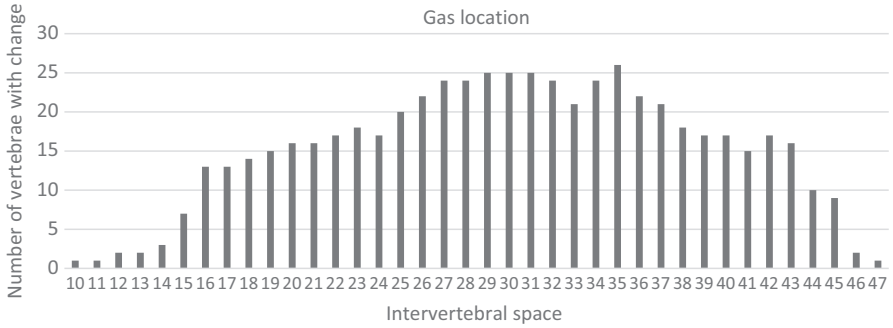

FIGURE 7 Distribution of gas accumulation along the vertebral column in fish examined by computed tomography. The horizontal axis depicts the vertebral number from the cranial to caudal direction. The vertical axis depicts the number of vertebrae with gas in the notochord caudal to the specified vertebra

TABLE 3 Visually normal and short fish from the four locations (N = 60) with histories of affected fish. Radiographic diagnoses of normal, mild, moderate, and marked changes are summarized

	Mean body length in cm (no. of affected vertebrae)			
Visual category	**Normal**	**Mild**	**Moderate**	**Marked**
Normal	70.5 (0)	69.1 (12.5)	66.5 (13.8)	64.8 (28)
Short	—	—	60.0 (17)	56.7 (36.8)

Note: Mean body length in cm and mean number of affected vertebrae (in parentheses) are shown within each category.

TABLE 4 Mean body length in cm with range (from snout to the base of the fin) within each of the four locations with histories of affected fish, N = number of individuals at each location

Category by visual inspection and radiographic diagnosis	Mean body length (range), cm			
	Location 1, N = 20	**Location 2, N = 15**	**Location 3, N = 15**	**Location 4, N = 10**
Short with curved cross-stitch	52.9 (49.6–58) N = 10	55.3 (53–60.5) N = 5	62 (58.1–65.8) N = 5	61.7 (57.4–66.4) N = 5
Visually long with curved cross-stitch	69.3 (67–70) N = 5	65.5 (59.5–72) N = 6	68.3 (67–70.5) N = 10	64.5 (61.7–67.3) N = 2
Normal	71.2 (69.8–73.2) N = 5	69.7 (69–70.2) N = 4	None	70.3 (68.3–71.7) N = 3

Note: Fish with curved cross-stitch deformities are grouped into visually normal and visibly short.

changes consistent with platyspondyly in the same individuals may suggest that these represent two different manifestations of one condition. On the other hand, there were important differences. In platyspondyly, altered opposing endplates mirror each other, and in some cases, the changes were limited to only the adjacent halves of neighbouring vertebral bodies. The changes were thus interpreted as emerging in intervertebral tissue. In the fish with curved cross-stitch, the opposing endplates did not mirror each other. Taken together with the observed perforations and inflammation in vertebral bodies, this strongly suggests a condition different from platyspondyly and may also suggest that the changes start in the vertebral bodies.

The metaplastic cartilage observed between the peripheries of curved endplates appeared similar to that previously described in the same location in salmon with platyspondyly (Kvellestad et al., 2000). In our study, we could not draw a conclusion about the sequential association between the four main types of changes, that is, curving, notochordal changes, including gas, perforations with prolapse or proliferations, and inflammation. One possible sequence is that the pathogenesis starts in the vertebral bodies followed by a reduced pressure in the notochordal tissue, resulting in displacement of the bodies, and finally altered growth directions in the endplates. In this interpretation, the metaplastic cartilage may represent an effort to stabilize the joints. The aetiology nevertheless remains unresolved, but if the pathological changes first occur in the vertebral bodies, it may be related to the cause of the inflammation.

Identification of individuals affected by curved cross-stitch vertebral deformity by external evaluation was challenging. According to our findings, there are no external characteristics that can reliably distinguish normal salmon from salmon with this deformity. Detection of radiographic and histologic changes in many fish (66%) with a normal external appearance demonstrated that the condition was more prevalent than indicated by external visual examination. These findings emphasize that external evaluation is an insufficient method for correct identification of vertebral deformities in salmons.

To our knowledge, this is the first study describing and recognizing a new entity with curved cross-stitch vertebrae as well as other associated changes. Similar radiographic changes occurred in fish in previous studies (G. Bæverfjord, pers. com.; Martens et al., 2005; Fjelldal et al., 2007). Gas could be detected and verified only by using CT; this may suggest that it was also present in the fish in those previous studies. The condition we described here may thus have existed for some years, but apparently at a lower prevalence than in recent years. Curved cross-stitch deformity was frequently present in our study populations, causing marked vertebral pathological changes. Further studies are encouraged to

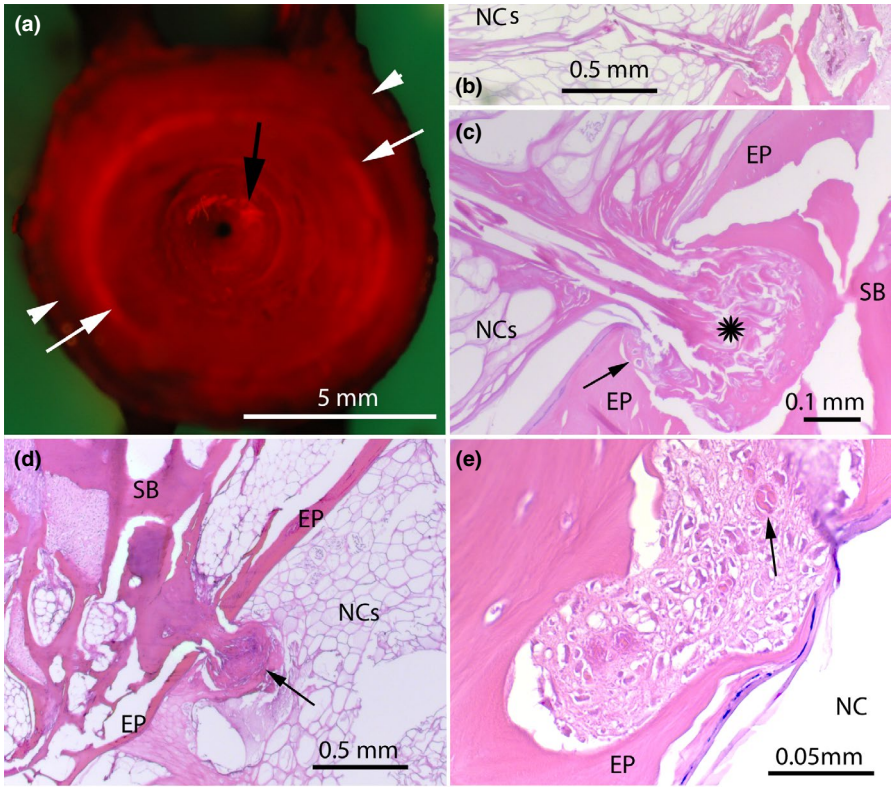

FIGURE 8 Pathological changes in the more axial parts of endplates (EPs). (a–c) Tissue of notochord cells (NCs) prolapsing through the endplate (EP) defects into the vertebral body's spongiotic bone (SB). (a) Whitish and filamentous material of NCs (black arrow). The curved peripheral rim extends between the white arrows and white arrowheads. Tissues were trypsinized, formalin-fixed, and stained with alizarin red. (b) The material in (a) is necrotic NCs that have prolapsed through the EP into the SB of the vertebral body. Detail from Figure 2(d), (c) slight amounts of chondroid tissue in the EP around the perforation (arrow). (d) A fibrovascular-like and fungal-shaped proliferation that appears necrotic, extending from the SB of the vertebra into the intervertebral space. (e) A putative early stage of the type of change depicted in (d), with a proliferation apparently penetrating the EP. Blood vessel (arrow)

FIGURE 9 Inflammation in altered vertebral bodies. (a) A cross-section through the middle (in the craniocaudal direction) of a body. The black spots contain melano-macrophages. Vertebral channel (Vc) with spinal cord. (b) Histology depicts increased cell numbers as well as melano-macrophages in fatty tissue between the trabeculae of the spongiotic bone (SB)

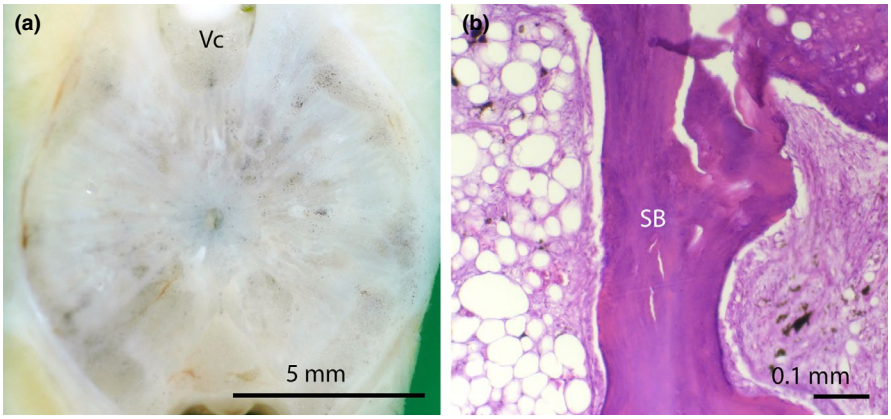

evaluate the aetiology, pathogenesis, and animal welfare concerns of this condition.

ACKNOWLEDGEMENTS

This research project "Prevention of the cross-stitch vertebrae syndrome in farmed Atlantic salmon" was funded by the Norwegian Seafood Research Fund (FHF), project no. 901430.

We are grateful to Dr. Grete Bæverfjord for leading the project and making this study possible. We also thank the slaughter plants and their staffs for access and for assistance with sampling, and the technical staff of the Faculty of Veterinary Medicine, Department of Companion Animal Clinical Sciences and Department of Basic Sciences and Aquatic Medicine, for assistance in radiographic examinations and processing of samples for histological examinations.

CONFLICT OF INTEREST

The authors declare that they have no competing interests.

ETHICAL APPROVAL

This study did not require official or institutional ethical approval. The animals were handled according to high ethical standards and national legislation.

DATA AVAILABILITY STATEMENT

The datasets used and/or analysed during the current study are available from the corresponding author on reasonable request.

ORCID

Cathrine Trangerud https://orcid.org/0000-0003-3767-5514
Erling Olaf Koppang https://orcid.org/0000-0003-4859-1455

REFERENCES

Abbas, J., Hamoud, K., Peled, N., & Hershkovitz, I. (2018). Lumbar Schmorl's nodes and their correlation with spine configuration and degeneration. *BioMed Research International*, *2018*, 1–9. https://doi.org/10.1155/2018/1574020

Aunsmo, A., Guttvik, A., Midtlyng, P. J., Larssen, R. B., Evensen, Ø., & Skjerve, E. (2008). Association of spinal deformity and vaccine-induced abdominal lesions in harvest-sized Atlantic salmon, *Salmo salar* L. *Journal of Fish Diseases*, *31*, 515–524. https://doi.org/10.1111/j.1365-2761.2007.00899.x

Aunsmo, A., Øvretveit, S., Breck, O., Valle, P. S., Larssen, R. B., & Sandberg, M. (2009). Modelling sources of variation and risk factors for spinal deformity in farmed Atlantic salmon using hierarchical- and cross-classified multilevel models. *Preventive Veterinary Medicine*, *90*, 137–145. https://doi.org/10.1016/j.prevetmed.2009.03.015

Baeverfjord, G., Antony Jesu Prabhu, P., Fjelldal, P. G., Albrektsen, S., Hatlen, B., Denstadli, V., … Waagbø, R. (2018). Mineral nutrition and bone health in salmonids. *Reviews in Aquaculture*, *11*(3), 740–765. https://doi.org/10.1111/raq.12255

Baeverfjord, G., Åsgård, T., & Shearer, K. D. (1998). Development and detection of phosphorus deficiency in Atlantic salmon, *Salmo salar* L., parr and post-smolts. *Aquaculture Nutrition*, *4*, 1–11. https://doi.org/10.1046/j.1365-2095.1998.00095.x

Bancroft, J. D., & Gamble, M. (2008). *Theory and practice of histological techniques*. London: Churchill Livingstone.

Belfquih, H., El Mostarchid, B., Akhaddar, A., Gazzaz, M., & Boucetta, M. (2014). Sciatica caused by lumbar epidural gas. *The Pan African Medical Journal*, *18*, 162–162. https://doi.org/10.11604/pamj.2014.18.162.1354

Berg, A., Rodseth, O. M., Tangeras, A., & Hansen, T. (2006). Time of vaccination influences development of adhesions, growth and spinal deformities in Atlantic salmon *Salmo salar*. *Diseases of Aquatic Organisms*, *69*, 239–248. https://doi.org/10.3354/dao069239

Berg, A., Yurtseva, A., Hansen, T., Lajus, D., & Fjelldal, P. G. (2012). Vaccinated farmed Atlantic salmon are susceptible to spinal and skull deformities. *Journal of Applied Ichthyology*, *28*, 446–452. https://doi.org/10.1111/j.1439-0426.2012.01988.x

Boglione, C., Gisbert, E., Gavaia, P., Witten, P. E., Moren, M., Fontagné, S., & Koumoundouros, G. (2013). Skeletal anomalies in reared European fish larvae and juveniles. Part 2: Main typologies, occurrences and causative factors. *Reviews in Aquaculture*, *5*, S121–S167. https://doi.org/10.1111/raq.12016

Fjelldal, P. G., Hansen, T. J., & Berg, A. E. (2007). A radiological study on the development of vertebral deformities in cultured Atlantic salmon (*Salmo salar* L.). *Aquaculture*, *273*, 721–728. https://doi.org/10.1016/j.aquaculture.2007.07.009

Fjelldal, P. G., Hansen, T., Breck, O., Ørnsrud, R., Lock, E.-J., Waagbø, R., … Eckhard Witten, P. (2012). Vertebral deformities in farmed Atlantic salmon (*Salmo salar* L.)—Etiology and pathology. *Journal of Applied Ichthyology*, *28*, 433–440. https://doi.org/10.1111/j.1439-0426.2012.01980.x

Fjelldal, P. G., Hansen, T., Breck, O., Sandvik, R., Waagbø, R., Berg, A., & Ørnsrud, R. (2009). Supplementation of dietary minerals during the early seawater phase increase vertebral strength and reduce the prevalence of vertebral deformities in fast-growing under-yearling Atlantic salmon (*Salmo salar* L.) smolt. *Aquaculture Nutrition*, *15*, 366–378. https://doi.org/10.1111/j.1365-2095.2008.00601.x

François, Y. (1966). Structure et développement de la vertèbre de Salmo et des téléostéens. *Archives De Zoologie Expérimentale Et Générale*, *107*, 283–326.

Gjerde, B., Pante, M. J. R., & Baeverfjord, G. (2005). Genetic variation for a vertebral deformity in Atlantic salmon (*Salmo salar*). *Aquaculture*, *244*, 77–87. https://doi.org/10.1016/j.aquaculture.2004.12.002

Gohil, I., Vilensky, J. A., & Weber, E. C. (2014). Vacuum phenomenon: Clinical relevance. *Clinical Anatomy*, *27*(3), 455–462. https://doi.org/10.1002/ca.22334

Grini, A., Hansen, T., Berg, A., Wargelius, A., & Fjelldal, P. G. (2011). The effect of water temperature on vertebral deformities and vaccine-induced abdominal lesions in Atlantic salmon, *Salmo salar* L. *Journal of Fish Diseases*, *34*, 531–546. https://doi.org/10.1111/j.1365-2761.2011.01265.x

Hansen, T., Fjelldal, P. G., Yurtseva, A., & Berg, A. (2010). A possible relation between growth and number of deformed vertebrae in Atlantic salmon (*Salmo salar* L.). *Journal of Applied Ichthyology*, *26*, 355–359. https://doi.org/10.1111/j.1439-0426.2010.01434.x

Haugarvoll, E., Bjerkås, I., Szabo, N. J., Satoh, M., & Koppang, E. O. (2010). Manifestations of systemic autoimmunity in vaccinated salmon. *Vaccine*, *28*, 4961–4969. https://doi.org/10.1016/j.vaccine.2010.05.032

Helland, S., Denstadli, V., Witten, P. E., Hjelde, K., Storebakken, T., Skrede, A., … Baeverfjord, G. (2006). Hyper dense vertebrae and mineral content in Atlantic salmon (*Salmo salar* L.) fed diets with graded levels of phytic acid. *Aquaculture*, *261*, 603–614. https://doi.org/10.1016/j.aquaculture.2006.08.027

Kvellestad, A., Høie, S., Thorud, K., Tørud, B., & Lyngøy, A. (2000). Platyspondyly and shortness of vertebral column in farmed Atlantic salmon *Salmo salar* in Norway-description and interpretation of pathologic changes. *Diseases of Aquatic Organisms*, *39*, 97–108. https://doi.org/10.3354/dao039097

Martens, L. G., Obach, A., Ritchie, G., & Witten, P. E. (2005). Analysis of a short tail phenotype in farmed Atlantic salmon (*Salmo salar*). *Fish Veterinary Journal*, *8*, 72–80.

McKay, L. R., & Gjerde, B. (1986). Genetic variation for a spinal deformity in Atlantic salmon, *Salmo salar*. *Aquaculture*, *52*, 263–272. https://doi.org/10.1016/0044-8486(86)90369-8

Müller, M. K., Ludewig, E., Oechtering, G., Scholz, M., & Flegel, T. (2013). The vacuum phenomenon in intervertebral disc disease of dogs based on computed tomography images. *Journal of Small Animal Practice*, *54*, 253–257. https://doi.org/10.1111/jsap.12063

Nordvik, K., Kryvi, H., Totland, G. E., & Grotmol, S. (2005). The salmon vertebral body develops through mineralization of two preformed tissues that are encompassed by two layers of bone. *Journal of Anatomy*, *206*, 103–114. https://doi.org/10.1111/j.1469-7580.2005.00372.x

Pfirrmann, C., & Resnick, D. (2001). Schmorl nodes of the thoracic and lumbar spine: Radiographic-pathologic study of prevalence, characterization, and correlation with degenerative changes of 1,650 spinal levels in 100 cadavers. *Radiology*, *219*, 368–374. https://doi.org/10.1148/radiology.219.2.r01ma21368

Samartzis, D., Mok, F. P. S., Karppinen, J., Fong, D. Y. T., Luk, K. D. K., & Cheung, K. M. C. (2016). Classification of Schmorl's nodes of the lumbar spine and association with disc degeneration: A large-scale population-based MRI study. *Osteoarthritis and Cartilage*, *24*, 1753–1760. https://doi.org/10.1016/j.joca.2016.04.020

Sugiura, S. H., Hardy, R. W., & Roberts, R. J. (2004). The pathology of phosphorus deficiency in fish—A review. *Journal of Fish Diseases*, *27*, 255–265. https://doi.org/10.1111/j.1365-2761.2004.00527.x

Sullivan, M., Guy, D. R., Roberts, R. J., & Manchester, N. J. (2007). The aetiology of spinal deformity in Atlantic salmon, *Salmo salar* L.: Influence of genetic factors on the frequency and severity in freshwater stages. *Journal of Fish Diseases*, *30*, 753–758. https://doi.org/10.1111/j.1365-2761.2007.00888.x

Sullivan, M., Hammond, G., Roberts, R. J., & Manchester, N. J. (2007). Spinal deformation in commercially cultured Atlantic salmon, *Salmo salar* L.: A clinical and radiological study. *Journal of Fish Diseases*, *30*, 745–752. https://doi.org/10.1111/j.1365-2761.2007.00889.x

Takle, H., Baeverfjord, G., Lunde, M., Kolstad, K., & Andersen, Ø. (2005). The effect of heat and cold exposure on HSP70 expression and development of deformities during embryogenesis of Atlantic salmon (*Salmo salar*). *Aquaculture*, *249*, 515–524. https://doi.org/10.1016/j.aquaculture.2005.04.043

Vågsholm, I., & Djupvik, H. O. (1998). Risk factors for spinal deformities in Atlantic salmon, *Salmo salar* L. *Journal of Fish Diseases*, *21*, 47–53. https://doi.org/10.1046/j.1365-2761.1998.00069.x

Wargelius, A., Fjelldal, P. G., & Hansen, T. (2005). Heat shock during early somitogenesis induces caudal vertebral column defects in Atlantic salmon (*Salmo salar*). *Development Genes and Evolution*, *215*, 350–357. https://doi.org/10.1007/s00427-005-0482-0

Weber, W. J., Berry, C. R., & Kramer, R. W. (1995). Vacuum phenomenon in twelve dogs. *Veterinary Radiology & Ultrasound*, *36*, 493–498. https://doi.org/10.1111/j.1740-8261.1995.tb00301.x

Witten, P. E., Gil-Martens, L., Hall, B. K., Huysseune, A., & Obach, A. (2005). Compressed vertebrae in Atlantic salmon *Salmo salar*: Evidence for metaplastic chondrogenesis as a skeletogenic response late in ontogeny. *Diseases of Aquatic Organisms*, *64*, 237–246. https://doi.org/10.3354/dao064237

Witten, P. E., Gil-Martens, L., Huysseune, A., Takle, H., & Hjelde, K. (2009). Towards a classification and an understanding of developmental relationships of vertebral body malformations in Atlantic salmon (*Salmo salar* L.). *Aquaculture*, *295*, 6–14. https://doi.org/10.1016/j.aquaculture.2009.06.037

Witten, P. E., Obach, A., Huysseune, A., & Baeverfjord, G. (2006). Vertebrae fusion in Atlantic salmon (*Salmo salar*): Development, aggravation and pathways of containment. *Aquaculture*, *258*, 164–172. https://doi.org/10.1016/j.aquaculture.2006.05.005

Ytteborg, E., Baeverfjord, G., Torgersen, J., Hjelde, K., & Takle, H. (2010). Molecular pathology of vertebral deformities in hyperthermic Atlantic salmon (*Salmo salar*). *BMC Physiology*, *10*, 12. https://doi.org/10.1186/1472-6793-10-12

How to cite this article: Trangerud C, Bjørgen H, Koppang EO, et al. Vertebral column deformity with curved cross-stitch vertebrae in Norwegian seawater-farmed Atlantic salmon, *Salmo salar* L.. *J Fish Dis*. 2020;43:379–389. https://doi.org/10.1111/jfd.13136